Research Paper
Computational Methods for Differential Equations
http://cmde.tabrizu.ac.ir
Vol. *, No. *, *, pp. 1-13
DOI:10.22034/cmde.2025.65032.2973

A new method for increasing the accuracy of the fifth-order WENO scheme

Hossein Mahmoodi Darian*

University of Tehran, College of Engineering, School of Engineering Science, Tehran, Iran.

Abstract

In this article, we introduce a new method for increasing the accuracy of the fifth-order WENO scheme. Recently, some methods were developed to increase the accuracy near discontinuities. We use the idea of these methods and the mapped WENO schemes to increase the accuracy both in smooth regions and near discontinuities. We also present some numerical experiments including the linear wave equation and Euler equations of gas dynamics to confirm the theoretical results. The results show that the introduced scheme attains better resolution at the smooth parts of the solution, while keeping the same non-oscillatory behavior of the WENO schemes at shocks and discontinuities.

Keywords. WENO schemes, Mapping function, Conservation laws.

2010 Mathematics Subject Classification. 65M22.

1. Introduction

Weighted essentially non-oscillatory (WENO) schemes are a class of high-order schemes used for solving problems which contain both smooth and discontinuous regions such as hyperbolic conservation laws. These schemes were first introduced in [15, 16]. For instance, the fifth-order WENO scheme is obtained by a convex weighted combination of three third-order stencils. In smooth regions the weights of these stencils are such that a fifth-order stencil is achieved, while near discontinuities the smoothest third-order stencil is selected. Gradually different modifications and improvements over the original scheme were proposed in the literature. Henrik et al. [14] introduced mapped WENO schemes (WENO-M). They noted that the fifth-order WENO method is only third-order accurate at critical points in smooth regions. They used a mapping function to the original weights so that the new weights satisfied the sufficient condition to achieve the optimal order of accuracy at or near critical points. This work made a basis for some other research [12, 13, 20, 22]. Recently, Amat et al. in a series of papers [5–9] introduced a new WENO interpolation capable of raising the order of accuracy close to discontinuities for some applications such as data interpolation and signal processing. Their idea was to use the highest-order stencil as long as the stencil does not contain any discontinuity. They used their new WENO algorithm for the numerical solution of conservation laws in [4], though the improvement over the classic WENO scheme is very small.

In this manuscript, we introduce a new method to improve the work of Amat et al. [4]. The idea is to use a combination of the third- and fourth-order smoothness indicators. Also, for further improvement a mapping function as in [14] is utilized to increase the accuracy in smooth regions and at the same time improve the accuracy near discontinuities. Also, to ensure the fifth-order accuracy for smooth solutions, the convergence order of the new schemes are numerically verified as it is customary in the literature of numerical solution of various partial differential equations [1–3, 11].

The manuscript is organized as follows. In section 2, we give a brief description of the WENO schemes and also the WENO-M scheme [14] and Amat et al. algorithm [4]. The main part of this work will be presented in section 3.

Received: 18 December 2024 ; Accepted: 07 October 2025.
∗ Corresponding author. Email: hmahmoodi@ut.ac.ir.

In section 4, the new scheme is assessed by numerical simulation of the linear advection equation and Euler equations of gas dynamics. Finally, the concluding remarks are given in section 5.

2. WENO schemes

In this section, we describe the WENO schemes for discretizing the governing equation of a conservation law. Consider the following equation:

$$u_t + f_x = 0, \tag{2.1}$$

where u is the conservative variable and $f = f(u)$ is the flux function. We consider a uniform grid in the x-direction and define the grid points as $x_i = i\Delta x$ where Δx is the grid size. The flux derivative is discretized in the conservative form as

$$f'(x_i) = \frac{f_{i+\frac{1}{2}} - f_{i-\frac{1}{2}}}{\Delta x} + O(\Delta x^m), \tag{2.2}$$

where $f_{i+\frac{1}{2}}$ is the numerical flux at $x_{i+\frac{1}{2}}$ and m is the order of the truncation error. In a $(2k-1)$th-order WENO scheme [15, 16], the flux $f_{i+\frac{1}{2}}$ is approximated such that $m = 2k-1$ in smooth regions and $m = k$ near discontinuities. This is done by a convex combination of k fluxes:

$$f_{i+\frac{1}{2}} = \sum_{r=0}^{k-1} \omega_r f_{i+\frac{1}{2}}^{(k,r)}\,, \qquad 0 \le r \le k-1, \tag{2.3}$$

where $f_{i+\frac{1}{2}}^{(k,r)}$ is a kth-order approximation of the flux. The flux $f_{i+\frac{1}{2}}^{(k,r)}$ satisfies (2.2) with $m = k$ by using the following stencil points

$$S_r^k = \{x_{i-r}, x_{i-r+1}, \cdots, x_{i-r+k-1}\}\,, \tag{2.4}$$

and it is obtained by a polynomial of degree at most $k-1$, $p_r^k(x)$, which its average in $[x_{j-\frac{1}{2}}, x_{j+\frac{1}{2}}]$ equals f_j for all $x_j \in S_r^k$:

$$f_j = \frac{1}{\Delta x}\int_{x_{j-\frac{1}{2}}}^{x_{j+\frac{1}{2}}} p_r^k(\xi)\, d\xi\,, \qquad x_j \in S_r^k. \tag{2.5}$$

The coefficients ω_r are nonlinear weights which determine the contribution of each $f_{i+\frac{1}{2}}^{(k,r)}$ to $f_{i+\frac{1}{2}}$. For consistency and stability, it is required:

$$\omega_r \ge 0\,, \qquad \sum_{r=0}^{k-1} \omega_r = 1. \tag{2.6}$$

In [15], the following weights, after extensive numerical experiments, are proposed

$$\omega_r = \frac{\alpha_r}{\sum_{q=0}^{k} \alpha_q}\,, \qquad \alpha_r = \frac{d_r}{(\beta_r + \epsilon)^2}, \tag{2.7}$$

where the coefficients d_r are optimal weights which generate the $(2k-1)$th-order central upwind scheme:

$$f_{i+\frac{1}{2}}^{(2k-1,k)} = \sum_{r=0}^{k-1} d_r f_{i+\frac{1}{2}}^{(k,r)}. \tag{2.8}$$

The coefficients β_r are called the smoothness indicators and defined by

$$\beta_r = \sum_{l=1}^{k-1} \int_{x_{i-\frac{1}{2}}}^{x_{i+\frac{1}{2}}} \Delta x^{2l-1} \left(\frac{\partial^l p_r^k(x)}{\partial x^l}\right)^2 dx. \tag{2.9}$$

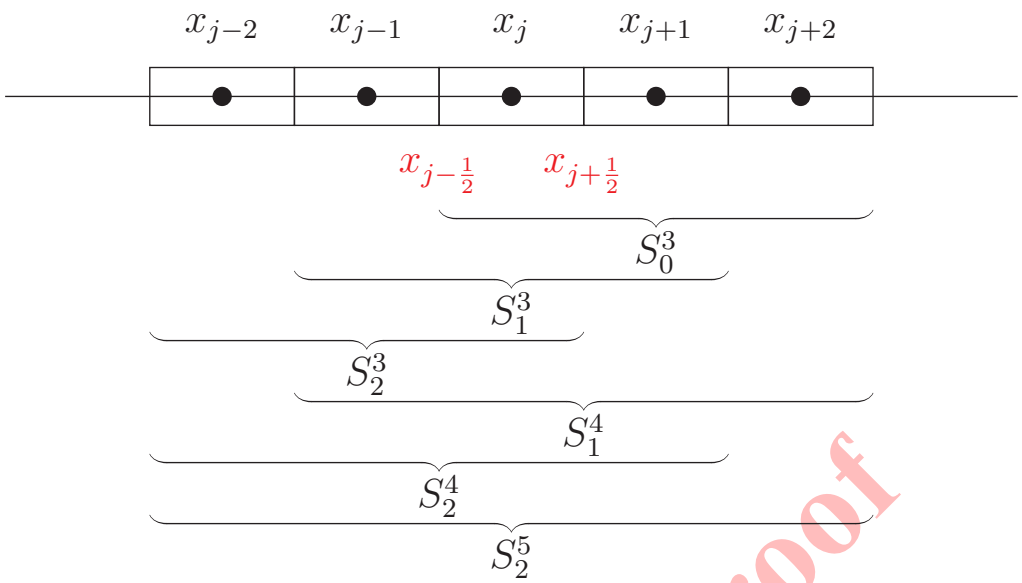

FIGURE 1. All sub-stencils inside S_2^5 ($k = 3$).

For the fifth-order scheme ($k = 3$), the optimal weights and third-order sub-stencils, shown by S_0^3, S_1^3 and S_2^3 in Fig. 1, are as follows

$$\begin{aligned} d_0 &= \frac{3}{10}, & f_{i+\frac{1}{2}}^{(3,0)} &= \frac{1}{6}(2f_j + 5f_{j+1} - f_{j+2}), \\ d_1 &= \frac{3}{5}, & f_{i+\frac{1}{2}}^{(3,1)} &= \frac{1}{6}(-f_{j-1} + 5f_j + 2f_{j+1}), \\ d_2 &= \frac{1}{10}, & f_{i+\frac{1}{2}}^{(3,2)} &= \frac{1}{6}(2f_{j-2} - 7f_{j-1} + 11f_j), \end{aligned} \tag{2.10}$$

and the smoothness-indicators are

$$\begin{aligned} \beta_0 &= \frac{13}{12}(f_j - 2f_{j+1} + f_{j+2})^2 + \frac{1}{4}(3f_j - 4f_{j+1} + f_{j+2})^2, \\ \beta_1 &= \frac{13}{12}(f_{j-1} - 2f_j + f_{j+1})^2 + \frac{1}{4}(f_{j-1} - f_{j+1})^2, \\ \beta_2 &= \frac{13}{12}(f_{j-2} - 2f_{j-1} + f_j)^2 + \frac{1}{4}(f_{j-2} - 4f_{j-1} + 3f_j)^2. \end{aligned} \tag{2.11}$$

Note that, according to [14], if the smoothness-indicators can be written as

$$\beta_r = B(1 + O(h^2)), \tag{2.12}$$

where B is some non-zero constant independent of r, then the scheme is fifth-order accurate in smooth regions. Taylor series expansion of smoothness indicators of (2.11) shows that

$$\beta_r = (hf_i')^2(1 + O(h^2)), \tag{2.13}$$

and therefore the fifth-order accuracy of the scheme in smooth regions is guaranteed.

2.1. **increasing the accuracy near discontinuities.** Amat et al. [4] proposed a method to utilize the available fourth-order schemes, i.e. S_1^4 and S_2^4 (see Fig. 1), near discontinuities. Before describing their main idea, we give the fourth-order schemes. Considering the cells involved in computing $f_{i+\frac{1}{2}}$ for the WENO5 scheme, there are two

fourth-order schemes which corresponding to stencils S_1^4 and S_2^4. Both the fourth-order schemes can be obtained by a linear combination of the third-order schemes:

$$f_{i+\frac{1}{2}}^{(4,1)} = \frac{1}{2} f_{i+\frac{1}{2}}^{(3,0)} + \frac{1}{2} f_{i+\frac{1}{2}}^{(3,1)},$$
$$f_{i+\frac{1}{2}}^{(4,2)} = \frac{3}{4} f_{i+\frac{1}{2}}^{(3,1)} + \frac{1}{4} f_{i+\frac{1}{2}}^{(3,2)}. \tag{2.14}$$

Also, the fifth-order central upwind scheme of (2.8) can be obtained by a linear combination of these fourth-order schemes:

$$f_{i+\frac{1}{2}}^{(5,2)} = \frac{2}{5} f_{i+\frac{1}{2}}^{(4,1)} + \frac{3}{5} f_{i+\frac{1}{2}}^{(4,2)}. \tag{2.15}$$

Now, if we define the vector of weights in (2.3) as $\mathbf{\Omega} = (\omega_0, \omega_1, \omega_2)$ and also define

$$\mathbf{C_1^4} = (0, \frac{3}{4}, \frac{1}{4}), \qquad \mathbf{C_2^4} = (\frac{1}{2}, \frac{1}{2}, 0), \qquad \mathbf{C_2^5} = (d_0, d_1, d_2) = (\frac{3}{10}, \frac{3}{5}, \frac{1}{10}), \tag{2.16}$$

then $\mathbf{\Omega} = \mathbf{C_1^4}$, $\mathbf{\Omega} = \mathbf{C_2^4}$, and $\mathbf{\Omega} = \mathbf{C_2^5}$ give $f_{i+\frac{1}{2}}^{(4,1)}$, $f_{i+\frac{1}{2}}^{(4,2)}$ and $f_{i+\frac{1}{2}}^{(5,2)}$, respectively. Also, note that

$$\mathbf{C_2^5} = D_1 \mathbf{C_1^4} + D_2 \mathbf{C_2^4}, \tag{2.17}$$

where

$$D_1 = \frac{2}{5}, \qquad D_2 = \frac{3}{5}. \tag{2.18}$$

In the WENO5 scheme if a discontinuity exists in any of the cells (Figure 1), then the scheme accuracy degrades from fifth- to third-order. In [4], the idea is to use one of the fourth-order schemes if the discontinuity is outside their corresponding stencil. Precisely, if a discontinuity is inside the rightmost cell (the cell centered at x_{j+2}) and the other four cells are smooth, then it is better to use the fourth-order scheme corresponding to sub-stencil S_2^4. This can be achieved if the optimal weights are $\mathbf{C_2^4}$ instead of $\mathbf{C_2^5}$. Similarly, if a discontinuity is inside the leftmost cell (the cell centered at x_{j-2}) and the other four cells are smooth, then it is better to use the fourth-order scheme corresponding to sub-stencil S_1^4 which can be achieved by using the optimal weights equal to $\mathbf{C_1^4}$ instead of $\mathbf{C_2^5}$. We denote these cases by I and II, respectively. To accomplish this, the optimal weights in (2.7), i.e. $\mathbf{C_2^5} = (d_0, d_1, d_2)$, is replaced by $\tilde{\mathbf{C}}_\mathbf{2}^\mathbf{5} = (\tilde{d}_0, \tilde{d}_1, \tilde{d}_2)$, where $\tilde{\mathbf{C}}_\mathbf{2}^\mathbf{5}$ is defined by replacing the constant coefficients D_1 and D_2 in (2.17) by new weights as

$$\tilde{\mathbf{C}}_\mathbf{2}^\mathbf{5} = W_1 \mathbf{C_1^4} + W_2 \mathbf{C_2^4}, \tag{2.19}$$

where

$$W_r = \frac{A_r}{A_1 + A_2}, \tag{2.20}$$

and

$$A_1 = \frac{D_1}{(\beta_2^{(4)} + \epsilon)^t}, \qquad A_2 = \frac{D_2}{(\beta_1^{(4)} + \epsilon)^t}, \tag{2.21}$$

where t is a positive number which should be greater than or equal to 2 for achieving the desired accuracy and $\beta_r^{(4)}$ is the smoothness indicators of the fourth-order stencils S_r^4 (see [10]):

$$\beta_r^{(4)} = \left(u_x + \frac{u_{x3}}{10}\right)^2 + \frac{13}{3} (u_{x2})^2 + \frac{781}{20} (u_{x3})^2, \tag{2.22}$$

where

$$
\begin{aligned}
r=1: \quad u_x &= \frac{1}{6}\left(-19f_{j-1}-33f_j+63f_{j+1}-11f_{j+2}\right),\\
u_{x2} &= \frac{1}{2}\left(f_{j-1}-2f_j+f_{j+1}\right),\\
u_{x3} &= \frac{1}{6}\left(-f_{j-1}+3f_j-3f_{j+1}+f_{j+2}\right),\\
r=2: \quad u_x &= \frac{1}{6}\left(11f_{j-2}-63f_{j-1}+33f_j+19f_{j+1}\right),\\
u_{x2} &= \frac{1}{2}\left(f_{j-1}-2f_j+f_{j+1}\right),\\
u_{x3} &= \frac{1}{6}\left(-f_{j-2}+3f_{j-1}j-3f_j+f_{j+1}\right).
\end{aligned}
$$

It should be mentioned that $\beta_2^{(4)}$ is used to obtain A_1 and $\beta_1^{(4)}$ is used to obtain A_2 and there is no typesetting error in (2.21). The accuracy condition (2.12) is also true for this scheme and since we have

$$\beta_r^{(4)} = (hf_i')^2(1+O(h^2)), \tag{2.23}$$

and therefore the fifth-order accuracy of this scheme in smooth regions is guaranteed. Now, it can be shown that for smooth regions (see [4]), we have

$$\tilde{\mathbf{C}}_{\mathbf{2}}^{\mathbf{5}} = \mathbf{C}_{\mathbf{2}}^{\mathbf{5}} + O(h^2), \tag{2.24}$$

and for cases I and II, we have

$$\begin{aligned}
&\text{Case I}: && \tilde{\mathbf{C}}_{\mathbf{2}}^{\mathbf{5}} = \mathbf{C}_{\mathbf{2}}^{\mathbf{4}} + O(h^{2t}),\\
&\text{Case II}: && \tilde{\mathbf{C}}_{\mathbf{2}}^{\mathbf{5}} = \mathbf{C}_{\mathbf{1}}^{\mathbf{4}} + O(h^{2t}).
\end{aligned}$$

2.2. **Mapped Weights.** Henrik et al. [14] showed that near the critical points (zero first-derivative), the original weights (2.7) are not close enough to their optimal values and cannot achieve the maximum accuracy. They introduced mapped WENO schemes (WENO-M) where the following mapping function is used to render the weights closer to their optimal values (d_r) so as to satisfy sufficient criteria for fifth-order convergence:

$$g_r(\omega) = \frac{\omega(d_r + d_r^2 - 3d_r\omega + \omega^2)}{d_r^2 + \omega(1-2d_r)}, \tag{2.25}$$

Since after mapping, the weights sum is no longer equal to unity, another normalization, similar to (2.7), is required

$$\tilde{\omega}_r = \frac{\tilde{\alpha}_r}{\sum_{q=0}^{k}\tilde{\alpha}_q}, \qquad \tilde{\alpha}_r = g_r(\omega_r), \tag{2.26}$$

and then $\tilde{\omega}_r$ are used instead of ω_r in (2.3).

3. New scheme

In this section, we introduce a new approach to use the fourth-order schemes for cases I and II. Through numerical experiments, we observed that we can improve [4] if we modify (2.21) as

$$
\begin{aligned}
A_1 &= \frac{D_1}{(\hat{\beta}_2+\epsilon)^t}, \qquad \hat{\beta}_2 = |\beta_2-\beta_1|,\\
A_2 &= \frac{D_2}{(\hat{\beta}_1+\epsilon)^t}, \qquad \hat{\beta}_1 = |\beta_0-\beta_1|,
\end{aligned} \tag{3.1}
$$

which only uses the third-order smoothness indicators (2.11). Specifically, $\beta_1^{(4)}$ and $\beta_2^{(4)}$ are replaced by $|\beta_0-\beta_1|$ and $|\beta_2-\beta_1|$, respectively. However, in smooth regions, Taylor series expansion [14] shows

$$\hat{\beta}_1 = (h^4 f_i' f_i''')(1+O(h)) , \qquad \hat{\beta}_2 = (h^4 f_i' f_i''')(1+O(h)),$$

which does not meet the accuracy condition (2.12). Therefore, we seek for a suitable combination of $\beta_r^{(4)}$ and $\hat{\beta}_r$ which can meet the accuracy condition. Through extensive numerical experiments, we found the following combination

$$\begin{aligned}
\hat{\beta}_1^{(4)} &= \max(\beta_1^{(4)}, C_1'|\beta_0-\beta_1|) , \qquad C_1' = C''\frac{\beta_2}{\beta_1^{(4)}+\epsilon},\\
\hat{\beta}_2^{(4)} &= \max(\beta_2^{(4)}, C_2'|\beta_2-\beta_1|), \qquad C_2' = C''\frac{\beta_0}{\beta_2^{(4)}+\epsilon},
\end{aligned} \tag{3.2}$$

where C'' is a positive constant for tuning. This combination recovers the accuracy condition (2.12) and then (2.24). Therefore, for the new scheme, we have

$$A_1 = \frac{D_1}{(\hat{\beta}_2^{(4)}+\epsilon)^t} , \qquad A_2 = \frac{D_2}{(\hat{\beta}_1^{(4)}+\epsilon)^t}. \tag{3.3}$$

We denote this scheme by WENO5/4I.

3.1. **Further improvement by mapping.** If we use the mapping function (2.25) for the weights of WENO5/4I, the scheme can be further improved. Here, we use (2.25) to map the weights of WENO5/4I toward $\tilde{\mathbf{C}}_{\mathbf{2}}^{\mathbf{5}} = (\tilde{d}_0, \tilde{d}_1, \tilde{d}_2)$. This is done by replacing d_r with $\tilde{d}_r$ in the mapping function definition (2.25) as

$$\tilde{g}_r(\omega) = \frac{\omega(\tilde{d}_r + \tilde{d}_r^2 - 3\tilde{d}_r\omega + \omega^2)}{\tilde{d}_r^2 + \omega(1-2\tilde{d}_r)}, \tag{3.4}$$

and then the new weights are obtained by normalization (2.26). This makes the weights of WENO5/4I closer to $\mathbf{C_1^4}$ for case I, to $\mathbf{C_2^4}$ for case II and to $\mathbf{C_2^5}$ otherwise. This allows to have the advantages of both the WENO5/4I and mapped WENO methods. We denote this scheme by WENO5/4IM.

In the next section, the performance of the introduced methods are assessed by several numerical experiments.

4. Numerical experiment

In this section, we assess the numerical performance of the new WENO scheme. For all the problems, the third-order TVD Runge-Kutta scheme [17] is used for the time integration

$$\begin{aligned}
u^{(1)} &= u^n + \Delta t L(u^n),\\
u^{(2)} &= \frac{3}{4}u^n + \frac{1}{4}u^{(1)} + \frac{1}{4}\Delta t L(u^{(1)}),\\
u^{n+1} &= \frac{1}{3}u^n + \frac{2}{3}u^{(2)} + \frac{2}{3}\Delta t L(u^{(2)}),
\end{aligned} \tag{4.1}$$

where Δt is the time-step. Also, we set $\epsilon = 10^{-12}$. The results of the mapped scheme (section 2.2) and the scheme of Amat et al (section 2.1) are labeled by WENO5M and WENO5/4, respectively. For WENO5/4 and WENO5/4I the power parameter is $t=2$. For WENO5/4IM since the mapping function quickly recovers the optimal weights we use $t=1$. Also, we set $C''=4$ for WENO5/4I and $C''=20$ for WENO5/4IM.

4.1. **Advection equation.** For the first test case, we consider is the linear wave or advection equation in $x\in[-1,1]$ with periodic boundary conditions:

$$u_t + u_x = 0, \qquad x\in[-1,1]. \tag{4.2}$$

First, we assess the error and convergence of the new schemes for a smooth solution. A periodic function in $\in[-1,1]$ is considered: $u(x,0)=\sin(\pi x)$. Since the time integration method is third-order, the time step is chosen to be $\Delta t = 8(\Delta x)^{\frac{5}{3}}$ in order that the error for the overall scheme is a measure of the spatial convergence only. The error

of the numerical solution is computed by comparing with the exact solution at $t = 2$. Table 1 shows the L_1 norm of the error:

$$L_1 = \frac{2}{N}\sum_{i=0}^{N} |u_i - u_{\text{exact},i}|\,, \tag{4.3}$$

For the sake of comparison, the results of the central upwind scheme (i.e. the optimal scheme), are given in the table. The results show both WENO5/4I and WENO5/4IM converge at fifth-order.

TABLE 1. Convergence properties of the new schemes.

	WENO5/4I		WENO5/4IM		Central Upwind	
Δx	L_1	Order	L_1	Order	L_1	Order
0.5^3	4.1659×10^{-3}	$--$	9.5659×10^{-4}	$--$	6.0250×10^{-4}	$--$
0.5^4	1.3365×10^{-4}	4.96	1.9610×10^{-5}	5.61	1.9480×10^{-5}	4.95
0.5^5	4.2237×10^{-6}	4.98	6.1817×10^{-7}	4.98	6.1797×10^{-7}	4.98
0.5^6	1.3268×10^{-7}	4.99	1.9450×10^{-8}	4.99	1.9449×10^{-8}	4.99
0.5^7	4.1609×10^{-9}	4.99	6.1141×10^{-10}	4.99	6.1140×10^{-10}	4.99

For investigating the performance of the new schemes around non-smooth regions, the initial condition is taken to be a function containing a Gaussian-, a triangle-, a square- and a half-ellipse-wave region [15]:

$$u(x,0) = \begin{cases} \frac{1}{6}(Q(x,\beta,\zeta-\delta) + Q(x,\beta,\zeta+\delta) + 4Q(x,\beta,\zeta)), & x \in [-0.8,-0.6], \\ 1, & x \in [-0.4,-0.2], \\ 1 - |10(x-0.1)|, & x \in [0.0,0.2], \\ \frac{1}{6}(R(x,\alpha,a-\delta) + R(x,\alpha,a+\delta) + 4R(x,\alpha,a)), & x \in [0.4,0.6], \\ 0, & \text{Otherwise.} \end{cases} \tag{4.4}$$

where

$$Q(x,\beta,\zeta) = \exp(-\beta(x-\zeta)^2),$$
$$R(x,\alpha,a) = \sqrt{\max(1-\alpha^2(x-a)^2, 0)},$$

and the constants are

$$a = 0.5\,, \quad \zeta = -0.7\,, \quad \delta = 0.005\,, \quad \alpha = 10\,, \quad \beta = \ln 2/(36\delta^2).$$

Figure 2 compares the results of different schemes at $t = 8$ which corresponds to four time periods. The number of grid points is $N = 201$ and the time-step is $\Delta t = 0.1$. The exact solution is also given. For better comparison, a closer views of the square and gaussian waves are given in Figure 3. The results of WENO5/4I is considerably more accurate than those of WENO5/4. Also, the results of WENO5/4IM is slightly more accurate than those of WENO5M.

To have a more clear view of the difference between the methods, we present the results at a very long time. Figure 4 compares the results of different schemes at $t = 100$ which corresponds to 50 time periods. This figure clearly shows the difference of the results. For the square wave, WENO5/4IM has the most accurate results. The WENO5M scheme ruins the shape of the square wave while the WENO5/4 and WENO5/4I schemes better preserve the shape of this wave. Furthermore, in the regions between two consecutive waves, we observe again the most accurate results belong to the WENO5/4IM scheme.

Since WENO schemes are nonlinear, the comparison of different schemes may lead to different conclusions in different solution times. Therefore, it is better to compare the error of different schemes at several solution times. For this reason, in Figure 5 the L_1 error of the schemes as a function of time for each of the four waves in logarithmic scale are plotted. The errors are computed at each complete time period (multiples of $T = 2$). Since the interval length of all the waves in (4.4) is 0.2, for each wave we consider an interval of length 0.4 centered at that wave to compute the L_1 error. The figure clearly shows for all the waves the least error belongs to WENO5/4IM. The exception is for the

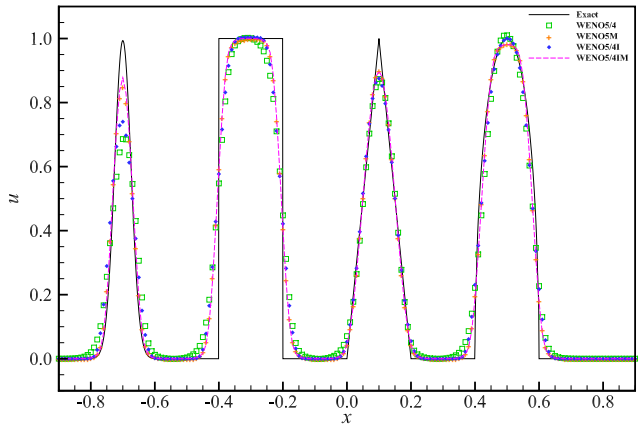

FIGURE 2. Numerical solution of the advection equation using $N = 201$ at $t = 8$.

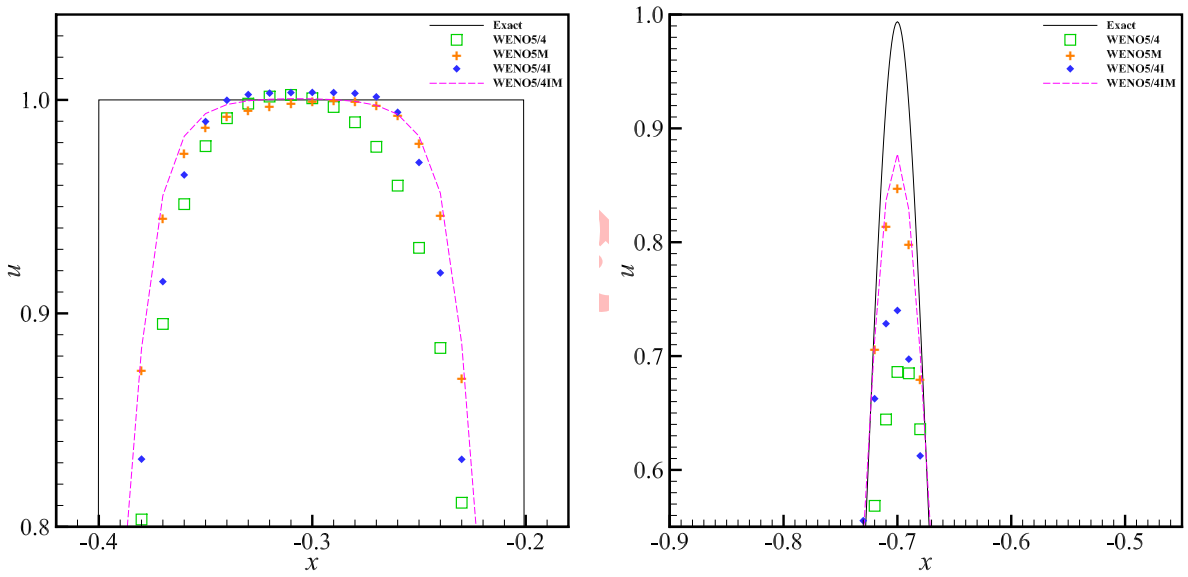

FIGURE 3. Closer view of the square (left) and gaussian (right) waves at $t = 8$.

triangle wave where in some solution times ($t < 20$) WEON5/4I has the least error. Also, for all the waves, the error of WENO5/4I is significantly smaller than those of WENO5/4.

4.2. **Shock-tube problem.** The second test case is the Sod shock-tube problem [19]. The governing equations are the one-dimensional Euler equations of gas dynamics:

$$U_t + F_x = 0, \quad U = \begin{pmatrix} \rho \\ \rho u \\ E \end{pmatrix}, \quad F = \begin{pmatrix} \rho u \\ \rho u^2 + p \\ (E + p)u \end{pmatrix}, \tag{4.5}$$

$$E = \rho(e + \frac{u^2}{2}), \quad p = \rho e(\gamma - 1), \quad \gamma = 1.4,$$

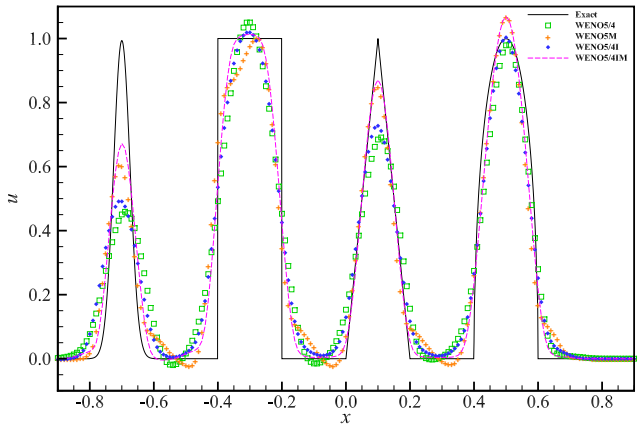

FIGURE 4. Numerical solution of the advection equation using $N = 201$ at $t = 100$.

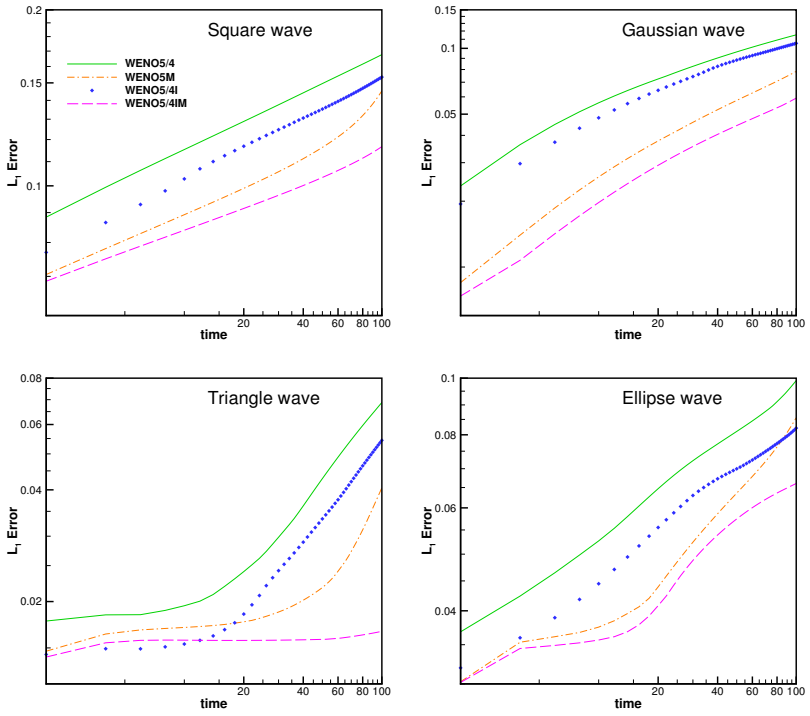

FIGURE 5. Numerical solution of the advection equation using $N = 201$ at $t = 100$.

where u, ρ, p and e denote the velocity, density, pressure and internal energy per unit mass, respectively. The solution domain is $[0, 10]$ and the left and right states of the discontinuity at $t = 0$ are

$$\begin{aligned} (\rho_L, u_L, p_L) &= (1, 0, 1), \qquad x \leq 5, \\ (\rho_R, u_R, p_R) &= (0.125, 0, 0.1), \qquad x > 5, \end{aligned} \tag{4.6}$$

where the exact solution possesses a self-similar solution which consists of a shock, a contact discontinuity and an expansion fan.

Figure 6 shows the density profile at $t = 2$ for different fifth-order schemes. At this time, the shock and contact discontinuity approximate locations are $x = 8.5$ and $x = 6.85$, respectively. Also, the expansion fan is approximately spanned from $x = 2.65$ fo $x = 4.85$. The grid spacing is $\Delta x = 0.05$ (201 points) and the time marching is done using a fixed time-step of $\Delta t = 0.01$. The characteristic-wise Lax-Friedrichs flux splitting [21] is used to handle both the negative and positive wave speeds. Although the difference between te results of the different schemes are small, we observe the most accurate results in all the regions belong to WENO5M. The difference between the results of WENO5M and WENO5/4IM are very small. The least accurate results belong to WENO5/4. Overall, one mas say the WENO5/4IM scheme can preserve both the advantages of the WENO5M and WENO5/4I schemes.

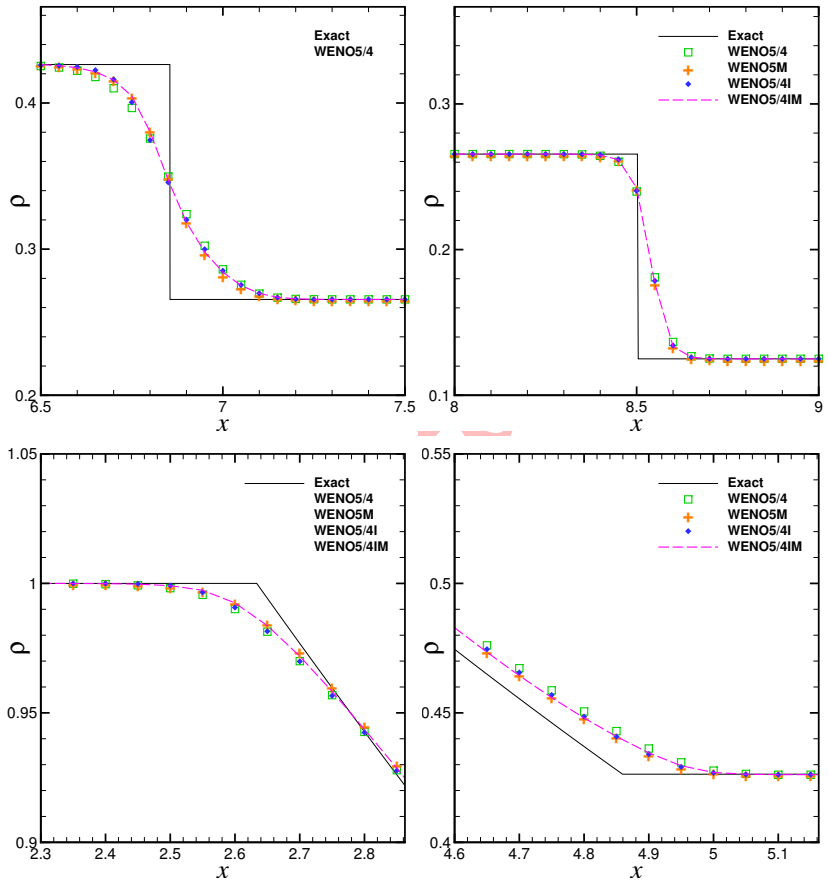

FIGURE 6. Shock-tube problem; Numerical solution at $t = 2$ with $N = 201$.

4.3. **Shock-density wave interaction.** This test case involves the interaction between a Mach 3 moving shock and a density wave in shape of a sine function [18]. The governing equations are the Euler Equations (4.5). The solution domain is $[-5, 5]$ and the initial states of the gas are as follows

$$(\rho_L, u_L, p_L) = \left(\frac{27}{7}, \frac{4\sqrt{35}}{9}, \frac{31}{3}\right), \qquad x \le -4, \tag{4.7}$$
$$(\rho_R, u_R, p_R) = (1 + 0.2\sin(5x), 0, 1), \qquad x > -4.$$

Figure 7 shows the exact density profile at $t = 1.8$. During the interaction, several shocks and high gradient regions appear. Specifically, at the time shown in the figure, the location of the moving shock is $x \approx 2.4$ and some shocks and steepening gradients are formed behind in $x \in [-2.9, 0.8]$. Also, during the interaction, the steepening gradients gradually form shocks. At $t = 1.8$, two of these steepening gradients at $x \approx -2.6$ and $x \approx -1.6$, already become discontinuous.

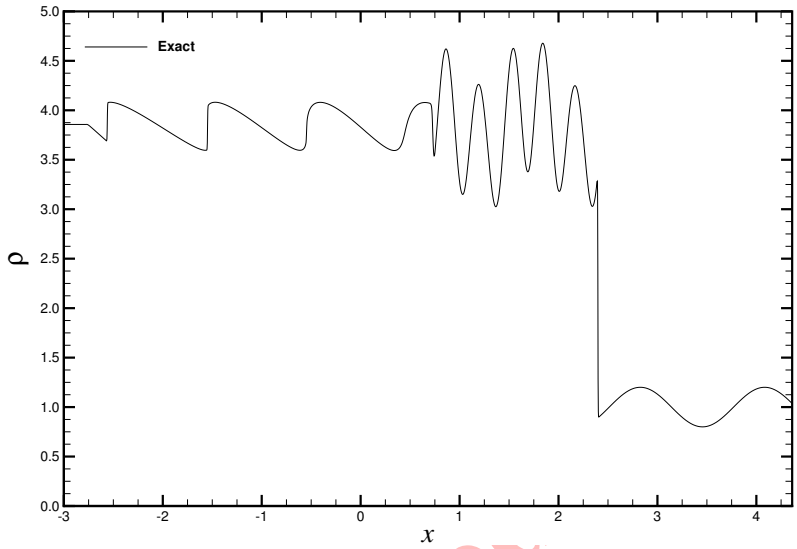

FIGURE 7. Shock-density wave interaction; Exact solution at $t = 1.8$.

Figure 8 compares the density distribution using $N = 201$ points ($\Delta x = 0.05$) for different schemes in the high gradient region. Also, the time-step is $\Delta t = 0.002$. The results show the most accurate results belong to WENO5/4IM and then WENO5M. Also, WENO5/4I gives more accurate results than WENO5/4. Again, we may say the WENO5/4IM scheme can preserve both the advantages of the WENO5M and WENO5/4I schemes.

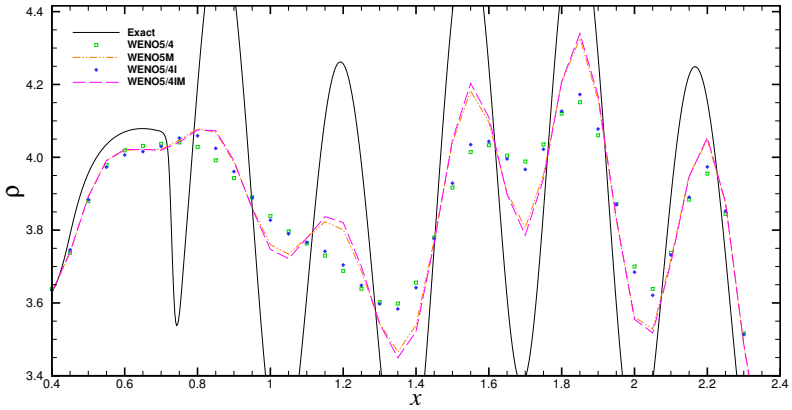

FIGURE 8. Shock-density wave interaction; Numerical solution using at $t = 1.8$ with $N = 201$.

5. Conclusion

In this article, we introduced a new fifth-order WENO scheme which was designed by improvement of a the WENO5/4 scheme [4]. The new scheme was denoted by WENO5/4I. Also, the this scheme was further improved by using a mapping function which was denoted by WENO5/4IM.

We examined the new schemes (WENO5/4I and WENO5/4IM) for the linear wave equation and also the Euler equations of gas dynamics. In all the test cases, the numerical results verified that WENO5/4I is considerably more accurate than WENO5/4. Also, the results verified that the WENO5/4IM scheme had the advantages of both the WENO5M scheme in smooth regions and the WENO5/4I scheme near discontinuities.

Acknowledgment

The authors would like to thank the University of Tehran for financial support of this project.

References

[1] D. Ahmadian and L. Ballestra, *The finite element method: A high-performing approach for computing the probability of ruin and solving other ruin-related problems*, Mathematical Methods in the Applied Sciences, *44*(13) (2021), 10353–10376.

[2] D. Ahmadian, L. Ballestra, and N. Karimi, *An extremely efficient numerical method for pricing options in the Black–Scholes model with jumps*, Mathematical Methods in the Applied Sciences, *44*(3) (2020), 2213–2236.

[3] D. Ahmadian, A. Ebrahimi, K. Ivaz, and M. Milev, *An investigation on the existence and uniqueness analysis of the optimal exercise boundary of American put option*, Filomat, *35*(4) (2021), 1095–1105.

[4] S. Amat, A. Baeza, J. Ruiz, and C. W. Shu, *On a new centered strategy to control the accuracy of weighted essentially non oscillatory algorithm for conservation laws close to discontinuities*, Numerical Methods for Partial Differential Equations, *37*(1) (2021), 172–195.

[5] S. Amat, J. Ruiz, and C. W. Shu, *On new strategies to control the accuracy of weno algorithms close to discontinuities*, SIAM Journal on Numerical Analysis, *57*(3) (2019), 1205–1237.

[6] S. Amat, J. Ruiz, and C. W. Shu, *On a new WENO algorithm of order 2r with improved accuracy close to discontinuities*, Applied Mathematics Letters, *105* (2020), 106285.

[7] S. Amat, J. Ruiz, and C. W. Shu, *On new strategies to control the accuracy of WENO algorithm close to discontinuities II: Cell averages and multiresolution*, Journal of Computational Mathematics, *38*(4) (2020), 661–682.

[8] S. Amat, J. Ruiz-Álvarez, C. W. Shu, and D. F. Yáñez, *Cell-average WENO with progressive order of accuracy close to discontinuities with applications to signal processing*, Applied Mathematics and Computation, *403* (2021), 126201.

[9] S. Amat, J. Ruiz-Álvarez, C. W. Shu, and D. F. Yáñez, *On the approximation of derivative values using a WENO algorithm with progressive order of accuracy close to discontinuities*, Computational and Applied Mathematics, *41*(6) (2022), 255.

[10] D. S. Balsara and C. W. Shu, *Monotonicity preserving weighted essentially non-oscillatory schemes with increasingly high order of accuracy*, Journal of Computational Physics, *160*(2) (2000), 405–452.

[11] O. Farkhonderooz and D. Ahmadian, *Mean-square stability of a constructed third-order stochastic Runge–Kutta schemes for general stochastic differential equations*, Computational Methods for Differential Equations, *10*(3) (2022), 617–638.

[12] H. Feng, F. Hu, and R. Wang, *A new mapped weighted essentially non-oscillatory scheme*, Journal of Scientific Computing, *51*(2) (2012), 449–473.

[13] H. Feng, C. Huang, and R. Wang, *An improved mapped weighted essentially non-oscillatory scheme*, Applied Mathematics and Computation, *232* (2014), 453–468.

[14] A. K. Henrick, T. D. Aslam, and J. M. Powers, *Mapped weighted essentially non-oscillatory schemes: Achieving optimal order near critical points*, Journal of Computational Physics, *207*(2) (2005), 542–567.

[15] G. S. Jiang and C. W. Shu, *Efficient implementation of weighted ENO schemes*, Journal of Computational Physics, *126*(1) (1996), 202–228.

[16] X. D. Liu, S. Osher, and T. Chan, *Weighted essentially non-oscillatory schemes*, Journal of Computational Physics, *115*(1) (1994), 200–212.
[17] C. W. Shu and S. Osher, *Efficient implementation of essentially non-oscillatory shock-capturing schemes*, Journal of Computational Physics, *77*(2) (1988), 439–471.
[18] C. W. Shu and S. Osher, *Efficient implementation of essentially non-oscillatory shock-capturing schemes, II*, Journal of Computational Physics, *83*(1) (1989), 32–78.
[19] G. A. Sod, *A survey of several finite difference methods for systems of nonlinear hyperbolic conservation laws*, Journal of Computational Physics, *27*(1) (1978), 1–31.
[20] U. S. Vevek, B. Zang, and T. H. New, *Adaptive mapping for high order WENO methods*, Journal of Computational Physics, *381* (2019), 162–188.
[21] C. W. Shu, *Essentially non-oscillatory and weighted essentially non-oscillatory schemes for hyperbolic conservation laws*, In: A. Iserles, editor, *Advanced Numerical Approximation of Nonlinear Hyperbolic Equations*, Lecture Notes in Mathematics, vol 1697, Springer, Berlin, Heidelberg, 1998, pp. 325–432.
[22] R. Wang, H. Feng, and C. Huang, *A new mapped weighted essentially non-oscillatory method using rational mapping function*, Journal of Scientific Computing, *67*(2) (2016), 540–580.